npj | climate and atmospheric science

Article

Published in partnership with CECCR at King Abdulaziz University

https://doi.org/10.1038/s41612-025-01000-4

Shifting influences of Indian Ocean Dipole and western Pacific subtropical high on annual precipitation $\delta^{18}O$ in southern East Asia

Check for updates

Jingyi Zhang[1,2], Wusheng Yu[1] ✉, Lonnie G. Thompson[3], Stephen Lewis[4], Alexandre Cauquoin[5], Martin Werner[6], Zhaowei Jing[7], Yaoming Ma[1,8,9], Baiqing Xu[1], Guangjian Wu[1], Rong Guo[1,8], Pengjie Ren[1,8], Zhuanxia Zhang[1,8], Qiaoyi Wang[1,8] & Dongmei Qu[1]

Clarifying relationships between stable oxygen isotope ratios in precipitation ($\delta^{18}O_p$) and atmospheric circulations including the Indian Ocean Dipole (IOD) and western Pacific subtropical high (WPSH) forms the basis of paleocirculation reconstructions. However, whether the IOD and WPSH modulate interannual variations of $\delta^{18}O_p$ remains unclear. Here, we reveal the links between the IOD/WPSH and the annual $\delta^{18}O_p$ in southern East Asia. We found that the IOD strongly influenced annual $\delta^{18}O_p$ before 1999 by changes in moisture supply from different transport pathways and convection. However, the link became decoupled after 1999, resulting from the transition of the IOD from a symmetric to an asymmetric pattern. In contrast, significantly enhanced WPSH emerges as an important influence on annual $\delta^{18}O_p$ after 1999. Therefore, the IOD and WPSH alternately influence interannual variation of $\delta^{18}O_p$ around 1999. Our findings imply that signals of IOD and WPSH should be considered in different periods to better interpret paleoclimate records.

Precipitation is critical to the production and livelihood of more than 1.6 billion people in East Asia. It is a major contributor to water resources; however, an excess of rainfall triggers water disasters[1,2]. In this region, interannual changes in precipitation are closely related to the atmospheric circulations of the Pacific and Indian Oceans[3,4]. Hence, numerous studies have examined changes in the atmospheric circulations across this region[5,6]. As a fingerprint, stable oxygen isotope ratios ($\delta^{18}O$) recorded in East Asian speleothems[7–9], tree-rings[10–13], and deep-sea sediment cores[14–16] have been used to reconstruct the history of atmospheric circulations. However, the interpretation of these paleoclimate records is clouded by an incomplete understanding of the link between the $\delta^{18}O$ signals preserved in these records and the atmospheric circulations. In that regard, establishing the links between atmospheric circulations and annual precipitation $\delta^{18}O$ ($\delta^{18}O_p$) is essential for interpreting the $\delta^{18}O$ records preserved in the paleoclimate archives[17–25].

There have been a range of studies in southern East Asia that have attributed $\delta^{18}O_p$ variability to different atmospheric circulations. Some studies have discussed the relationships between annual $\delta^{18}O_p$ and the East Asian and Indian summer monsoons[26–31] and proposed the competitive influences of these monsoons on the $\delta^{18}O_p$[32–35]. However, apart from the monsoons, changes in annual $\delta^{18}O_p$ in southern East Asia have also been argued to be closely related to the westerlies, with higher $\delta^{18}O_p$ values associated with a southward-shifting westerly jet during the summer months[36]. Another group of studies has proposed that the El Niño Southern Oscillation (ENSO) controls the interannual variability of $\delta^{18}O_p$ in southern East Asia either by modulating the rainout intensity during moisture transport[30,35,37–39] or by causing changes in convection within the moisture source regions[40–43]. However, the influence of ENSO on annual $\delta^{18}O_p$ in southern East Asia is unstable[44]. Therefore, factors other than ENSO appear

[1]State Key Laboratory of Tibetan Plateau Earth System, Environment and Resources (TPESER), Institute of Tibetan Plateau Research, Chinese Academy of Sciences, Beijing, 100101, China. [2]College of Tourism, Henan Normal University, Xinxiang, 453007, China. [3]Byrd Polar and Climate Research Center, The Ohio State University, Columbus, OH, 43210, USA. [4]Catchment to Reef Research Group, Centre for Tropical Water and Aquatic Ecosystem Research, James Cook University, Townsville, QLD, 4811, Australia. [5]Institute of Industrial Science, The University of Tokyo, Kashiwa, Japan. [6]Alfred Wegener Institute (AWI), Helmholtz Centre for Polar and Marine Sciences, Bremerhaven, Germany. [7] School of Ecology and Nature Conservation, Beijing Forestry University, Beijing, 100083, China. [8]University of Chinese Academy of Sciences, Beijing, 100049, China. [9]College of Atmospheric Science, Lanzhou University, Lanzhou, 730000, China.
✉e-mail: yuws@itpcas.ac.cn

to impact the interannual variability of $\delta^{18}O_p$ in southern East Asia, and a systematic study is required to explore these additional factors that affect $\delta^{18}O_p$ variability in this region.

As an important mode of interannual climate variability in the Indian Ocean, the Indian Ocean Dipole (IOD) is generally acknowledged to have a considerable influence on the precipitation across large parts of the tropics and even in the relatively distal southern East Asia[45–47]. However, the role of the IOD on the $\delta^{18}O_p$ in southern East Asia has received less attention. Importantly, the frequency of extreme positive IOD events significantly increases under global warming, and these events likely have a considerable influence on $\delta^{18}O_p$ in southern East Asia[48,49]. However, whether the changes in IOD decouple its relationship with the annual $\delta^{18}O_p$ in southern East Asia is unknown. These knowledge gaps motivate a further investigation in southern East Asia on the relationship between the IOD and annual $\delta^{18}O_p$ and the stability of this relationship over time.

In the western Pacific, a permanent large-scale anticyclonic circulation system known as the western Pacific subtropical high (WPSH) develops over the middle and lower troposphere and strongly modulates the climate of southern East Asia[50–52]. Previous studies have focused on the effects of the WPSH on the $\delta^{18}O_p$ on seasonal timescales in southern East Asia and shown that, during the pre-monsoon season, the adjacent oceanic moisture driven by the WPSH causes relatively high $\delta^{18}O_p$ values over the region[53,54]. However, few studies have examined the influence of the WPSH on the $\delta^{18}O_p$ in southern East Asia on an interannual timescale. Moreover, several studies found that the frequency of strong WPSH events is also increasing under global warming[55,56]. However, the nature and strength of the relationship between the WPSH and the annual $\delta^{18}O_p$ in southern East Asia have not been assessed. Therefore, the role of the WPSH on the annual $\delta^{18}O_p$ in southern East Asia remains to be determined.

This study aims to identify the possible influences of the IOD and WPSH on the $\delta^{18}O_p$ in southern East Asia on interannual timescales. To achieve this, we first retrieve the observed $\delta^{18}O_p$ data in Hong Kong over the period 1961–2021 and modeled $\delta^{18}O_p$ data across southern East Asia over the period 1979–2020. We then clarify the linkages between the IOD and WPSH and the annual $\delta^{18}O_p$ in southern East Asia, respectively. Finally, we reveal the mechanisms of how the IOD and WPSH modulate annual $\delta^{18}O_p$ variability across southern East Asia.

Results

Relationships between $\delta^{18}O_p$ and IOD with WPSH

The interannual variations in the $\delta^{18}O_p$ at Hong Kong during 1961–2021, along with the DMI and WPSHII, are shown in Fig. 1. The $\delta^{18}O_p$ values show considerable interannual fluctuations, with the values ranging from −6.51‰ to −3.73‰ and a mean of −4.91‰ ± 0.61‰ (Fig. 1b, c). These data show that the trends in annual $\delta^{18}O_p$ at Hong Kong closely follow the DMI between 1961 and 1998 (Fig. 1b). Indeed, over this timeframe annual $\delta^{18}O_p$ is significantly and strongly correlated to the DMI, with a correlation coefficient of 0.49 ($n = 31$, $p < 0.01$) (Fig. 1b). However, the correlation in the subsequent 1999–2021 period breaks down and is not significant ($r = -0.09$, $n = 23$, $p = 0.70$) (Fig. 1b). That is, the interannual variations in the $\delta^{18}O_p$ at Hong Kong are remarkably linked to the IOD before 1999, but the linkage disappeared after 1999. Similar comparisons between the annual $\delta^{18}O_p$ and the WPSHII show opposite changes in the correlations during the two periods to those between the annual $\delta^{18}O_p$ and the DMI (Fig. 1c). Before 1999 the correlation coefficient between the annual $\delta^{18}O_p$ and the WPSHII

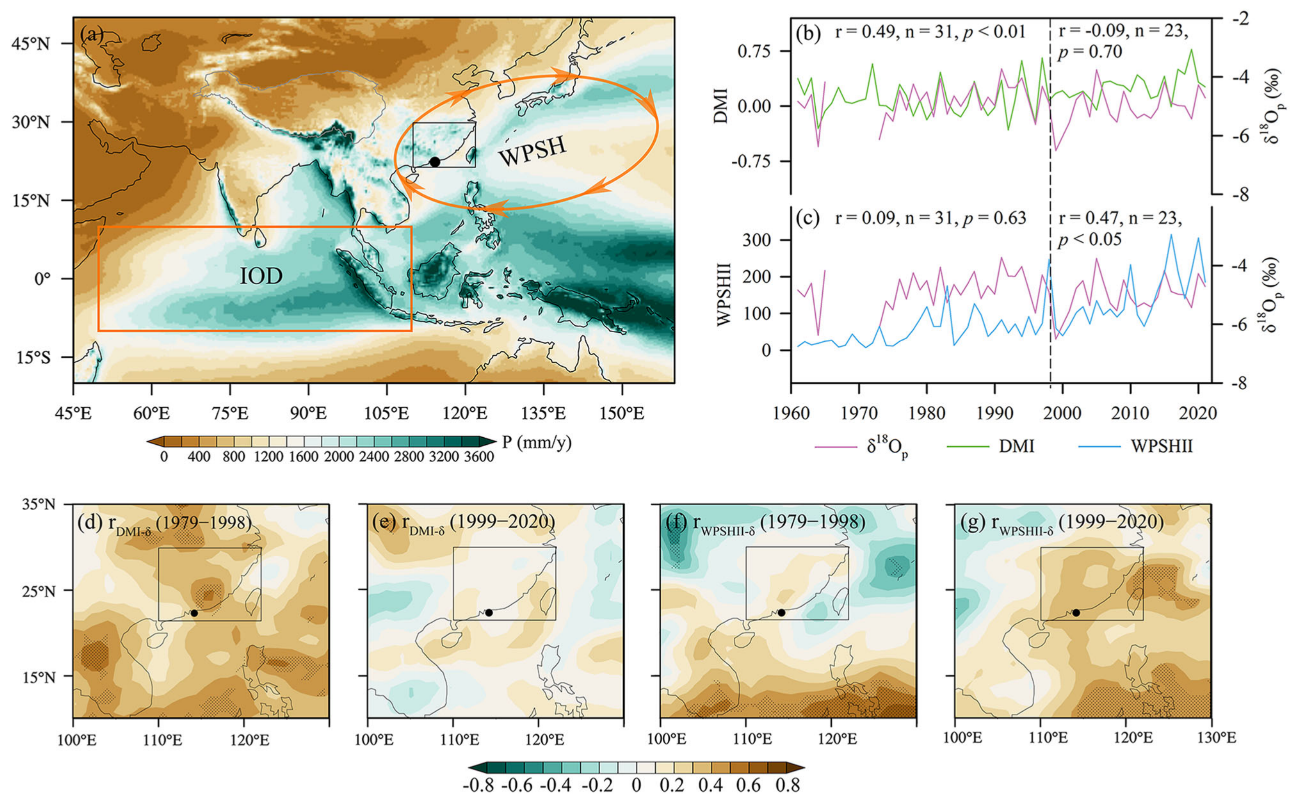

Fig. 1 | Location of Hong Kong and correlations between the DMI/WPSHII and the annual $\delta^{18}O_p$ at Hong Kong. **a** Map of southern East Asia (black rectangle) showing the location of Hong Kong (black dot). The colors show the spatial distributions of the mean annual precipitation amount (P) from 1961 to 2021. The orange box marks the region where the IOD occurs. The orange circle marks the major region where the WPSH occurs. **b**, **c** Interannual variations in the $\delta^{18}O_p$ at Hong Kong compared with DMI (**b**), and WPSHII (**c**) during 1961–2021. The black dashed vertical line divides the study period into 1961–1998 and 1999–2021. **d**–**g** Spatial distributions of the correlation coefficients between the DMI (**d**, **e**), WPSHII (**f**, **g**), and annual $\delta^{18}O_p$ of each grid point during 1979–1998 (**d**, **f**) and 1999–2020 (**e**, **g**), respectively. Dotted areas highlight correlations exceeding the 95% confidence level. The black dots indicate the location of Hong Kong, and the black rectangles mark the region of southern East Asia.

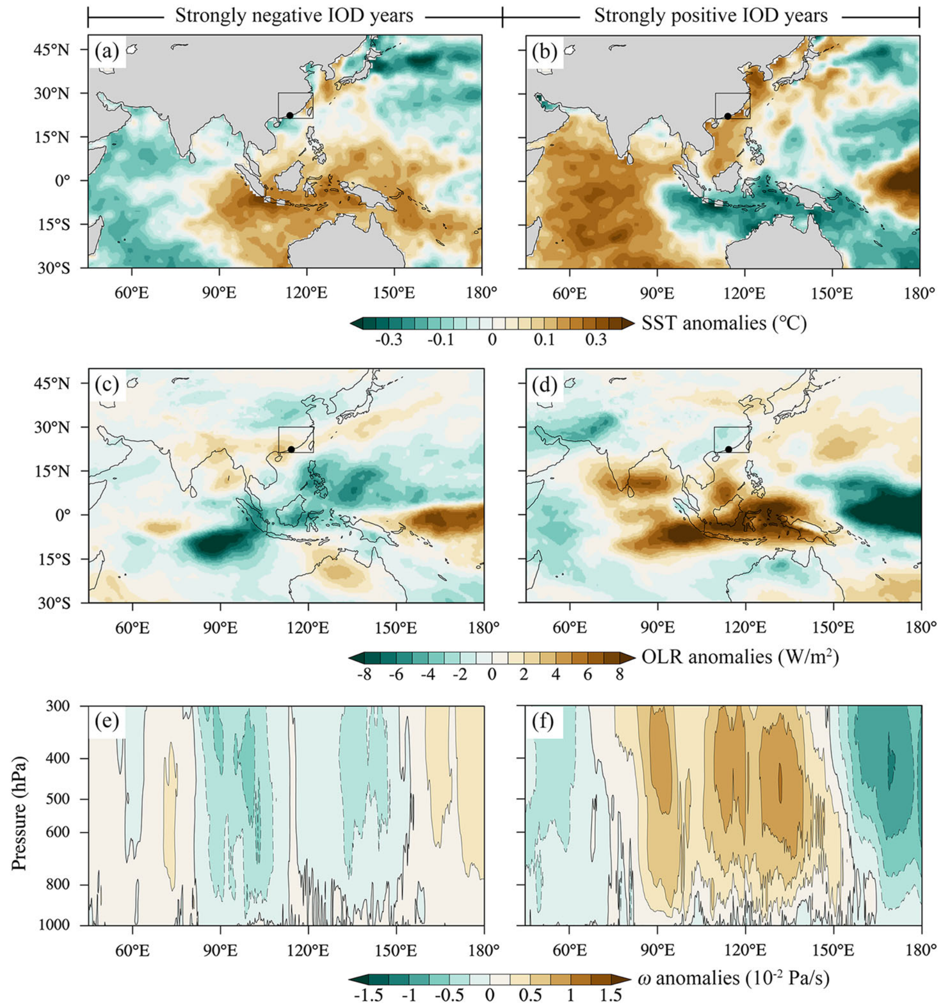

Fig. 2 | Spatial distributions of annual SST, OLR, and vertical velocity anomalies during the strongly negative and positive IOD years.
a, **b** Spatial distributions of annual SST anomalies during the strongly negative (**a**) and positive (**b**) IOD years. **c**, **d** Spatial distributions of annual OLR anomalies during the strongly negative (**c**) and positive (**d**) IOD years. The black dots indicate the location of Hong Kong, and the black rectangles mark the region of southern East Asia. **e**, **f** Vertical profiles of meridional mean vertical velocity (ω) anomalies for the latitude range 15°S–15°N during the strongly negative (**e**) and positive (**f**) IOD years. Negative and positive anomaly values for vertical velocity indicate rising and sinking motions, respectively. The anomalies are defined as the mean values during the strongly negative and positive IOD years subtracted by the mean values during 1961–1998, respectively.

is 0.09 ($n = 31$, $p = 0.63$), and it increases to 0.47 thereafter ($n = 23$, $p < 0.05$) (Fig. 1c). Therefore, the linkage between the annual $\delta^{18}O_p$ and the WPSH became significant after 1999, which was completely opposite to the role that the IOD played on the annual $\delta^{18}O_p$ at Hong Kong (Fig. 1b, c). It is clear that both the IOD and WPSH can affect the changes of annual $\delta^{18}O_p$ at Hong Kong, but those impacts reversed around 1999.

We further analyzed the spatial correlations between the DMI/WPSHII and the annual $\delta^{18}O_p$ from the ECHAM6-wiso outputs over a broader southern East Asia (grid points) during 1979–1998 and 1999–2020, respectively (Fig. 1d–g). Similar to the results from the Hong Kong station, the clear shift in the correlations between the DMI/WPSHII and the annual $\delta^{18}O_p$ is also strongly evident across broader southern East Asia. There are positive correlation coefficients between the DMI and the annual $\delta^{18}O_p$ in southern East Asia before 1999 which weaken thereafter (Fig. 1d, e), while the positive correlation coefficients between the WPSHII and the annual $\delta^{18}O_p$ become much stronger after 1999 than those during the 1979–1998 period (Fig. 1f, g). Therefore, the shifting influences of the IOD and WPSH on the annual $\delta^{18}O_p$ occur across the whole of southern East Asia.

Impact of IOD on annual $\delta^{18}O_p$

In light of the significant correlation between the IOD and annual $\delta^{18}O_p$ in southern East Asia, including Hong Kong station, which mainly appeared before 1999, we first consider how the IOD influenced the interannual variations in $\delta^{18}O_p$ in southern East Asia during the 1961–1998 period. We define the strongly negative and positive IOD years by the troughs and peaks of the DMI curve, respectively (Supplementary Fig. 1a). In this case, six strongly negative IOD years (1964, 1980, 1985, 1989, 1992, and 1996) and six strongly positive IOD years (1976, 1982, 1987, 1991, 1994, and 1997) were identified over the 1961–1998 period (Note that we have not considered the IOD events during 1966–1972, for there were no observed $\delta^{18}O_p$ data during this period).

During the strongly negative IOD years, the SSTs display positive anomalies in the Indo-Pacific Warm Pool and negative anomalies in the western tropical Indian Ocean (Fig. 2a). Those patterns in SST anomalies tend to strengthen convection in the Indo-Pacific Warm Pool and weaken convection in the western tropical Indian Ocean. Correspondingly, the opposite patterns in the spatial OLR anomalies between the Indo-Pacific Warm Pool (negative values) and the Western Tropical Indian Ocean (positive values) also demonstrate the strong convection in the Indo-Pacific Warm Pool and the weak convection in the Western Tropical Indian Ocean (Fig. 2c). The differences of convection in the two areas are favorable to enhance the Indian Ocean Walker circulation. The vertical velocity profiles clearly illustrate the changes in the Indian Ocean Walker circulation. As shown in Fig. 2e, the negative anomalies in the vertical velocity occur in the Indo-Pacific Warm Pool (80°E–150°E), including the eastern tropical Indian Ocean, while positive anomalies occur in the western tropical Indian Ocean and adjacent region (45°E–80°E). These results support that the stronger rising motion in the Indo-Pacific Warm Pool and the stronger sinking motion in the western tropical Indian Ocean enhance the Indian Ocean Walker circulation during the strongly negative IOD years.

Influenced by the enhanced Indian Ocean Walker circulation during the strongly negative IOD years, the moisture supplied from the equatorial Indian Ocean (southeastern side of the Indian Peninsula) to southern East Asia increases significantly (oval drawn with a solid pink line in Fig. 3a, c). On

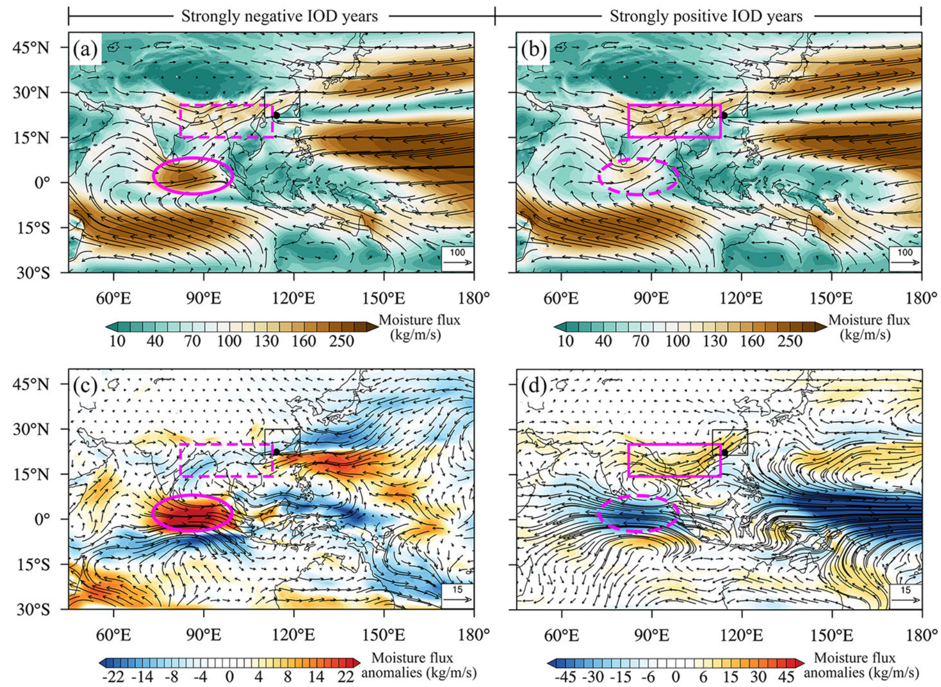

Fig. 3 | Atmospheric circulation patterns during the strongly negative and positive IOD years. Vertically integrated moisture flux fields (**a**, **b**) and moisture flux field anomalies (**c**, **d**) at 1000–500 hPa during the strongly negative (**a**, **c**) and positive (**b**, **d**) IOD years. The anomalies are defined as the mean values during the strongly negative and positive IOD years subtracted by the mean values during 1961–1998, respectively. The black dots indicate the location of Hong Kong, and the black rectangles mark the region of southern East Asia. The solid line circles or rectangles with pink mark the areas of increased moisture flux, and the dashed line circles or rectangles with pink mark the areas of decreased moisture flux.

the contrary, the contribution of moisture from the northern Bay of Bengal and northern Indochina Peninsula to southern East Asia relatively decreases (rectangle drawn with a dashed blue line in Fig. 3a, c). Therefore, the influence of the moisture from the equatorial Indian Ocean on the $\delta^{18}O_p$ in southern East Asia is stronger. It should be noted that the moisture supplied from the equatorial Indian Ocean is characterized by lower $\delta^{18}O_v$ values at 1000–500 hPa than the northern Bay of Bengal and northern Indochina Peninsula (Supplementary Fig. 2a), which provides a lower background value for the $\delta^{18}O_p$ in southern East Asia. In other words, the lower $\delta^{18}O_v$ values will significantly decrease the $\delta^{18}O_p$ in southern East Asia. In addition, the moisture supplied from the equatorial Indian Ocean to the study area has a relatively long transport pathway and a larger latitudinal deference. Hence, the $\delta^{18}O_v$ along the transport pathway experiences a stronger "rainout effect" and "latitude effect." As a consequence, the subsequent $\delta^{18}O_p$ in southern East Asia becomes lower (Fig. 4a). More importantly, when the moisture passes through the strong convective region of the Indo-Pacific Warm Pool, the enhanced convection and rising motion in the region uplifts the moisture from the near-surface to higher altitudes which enhances the recycling of moisture. The recycled moisture is isotopically depleted due to the rainout process[57,58] and could be advected toward the study area. Obviously, the enhanced convection further decreases the $\delta^{18}O_p$ values in southern East Asia (Fig. 4a). It is precisely because of the combined influences of the moisture supply and convection that the range of $\delta^{18}O_p$ values at Hong Kong during the strongly negative IOD years is as relatively as −4.36‰ to −6.38‰, with a mean of −5.09‰ (Figs. 1b, c and 4a).

During the strongly positive IOD years, however, the SST, OLR, and vertical velocity anomalies show the opposite patterns to those during the strongly negative IOD years (Fig. 2b, d, f). The results indicate that, under the influence of the strongly positive IOD events, the positive SST anomalies enhance convection and form the rising motion in the western tropical Indian Ocean, while the negative SST anomalies in the Indo-Pacific Warm Pool weaken convection and cause a sinking motion (Figs. 2b, d, f and 4b). This process leads to anomalous easterlies over the lower troposphere of the tropical Indian Ocean but anomalous westerlies over the upper troposphere of the tropical Indian Ocean (Fig. 4b). Clearly, the direction of the circulation caused by the strongly positive IOD events greatly weakens the Indian Ocean Walker circulation (Fig. 4b). In this case, the moisture contribution from the equatorial Indian Ocean to the study area is significantly reduced (ovals drawn with a dashed pink line in Fig. 3b, d). Meanwhile, more moisture from the northern Bay of Bengal and northern Indochina Peninsula is transported to southern East Asia (rectangles drawn with a solid pink line in Fig. 3b, d). The moisture supplied from the northern Bay of Bengal and northern Indochina Peninsula contains relatively high $\delta^{18}O_v$ (Supplementary Fig. 2b), which contributes to the relatively high background values for the $\delta^{18}O_p$ in southern East Asia. In addition, such moisture is transported to the study area via a relatively short transport pathway and experiences a relatively small latitude difference, leading to weaker isotopic depletion along the moisture transport pathway (Fig. 4b). Furthermore, the weaker convection and even a sinking motion occur within the upstream Indo-Pacific Warm Pool, which result in less recycling of moisture. This process also limits isotopic depletion in the study area during the strongly positive IOD years (Fig. 4b). As a result, $\delta^{18}O_p$ values at Hong Kong during the strongly positive IOD years ranging from −3.73‰ to −4.46‰, with the mean value of −4.13‰, which is 0.96‰ higher than that during the strongly negative IOD years (Figs. 1b, c and 4b).

Our results show that the influence of the IOD on the annual $\delta^{18}O_p$ in southern East Asia greatly reduced after 1999. Here, we discuss the causes of this major shift from correlation to non-correlation in the linkage between DMI and annual $\delta^{18}O_p$ in our study area around the year 1999. Over the 1961–1998 period, there were fluctuations in the DMI around zero, with some positive and negative phases (Supplementary Fig. 1a). These fluctuations indicate that the IOD was in a symmetrical phase during this period. The pattern of the IOD led to the Indian Ocean Walker circulation showing interannual differences between positive and negative IOD years, which contributed to the significant interannual variations of the $\delta^{18}O_p$ in southern East Asia. However, the DMI over the 1999–2021 period is characterized by an apparent increasing trend, and almost all DMI values are positive (Supplementary Fig. 1a). These results indicate that the IOD represents positive phases after 1999, and the IOD changed from a symmetric to asymmetric pattern. This transition of the IOD reduces the interannual variability of the Indian Ocean Walker circulation after 1999 and likewise the influence of the IOD on the annual $\delta^{18}O_p$ in southern East Asia. As a result, the annual $\delta^{18}O_p$ variations in southern East Asia are decoupled from the changes in IOD during the period 1999–2021 (Fig. 1b, e).

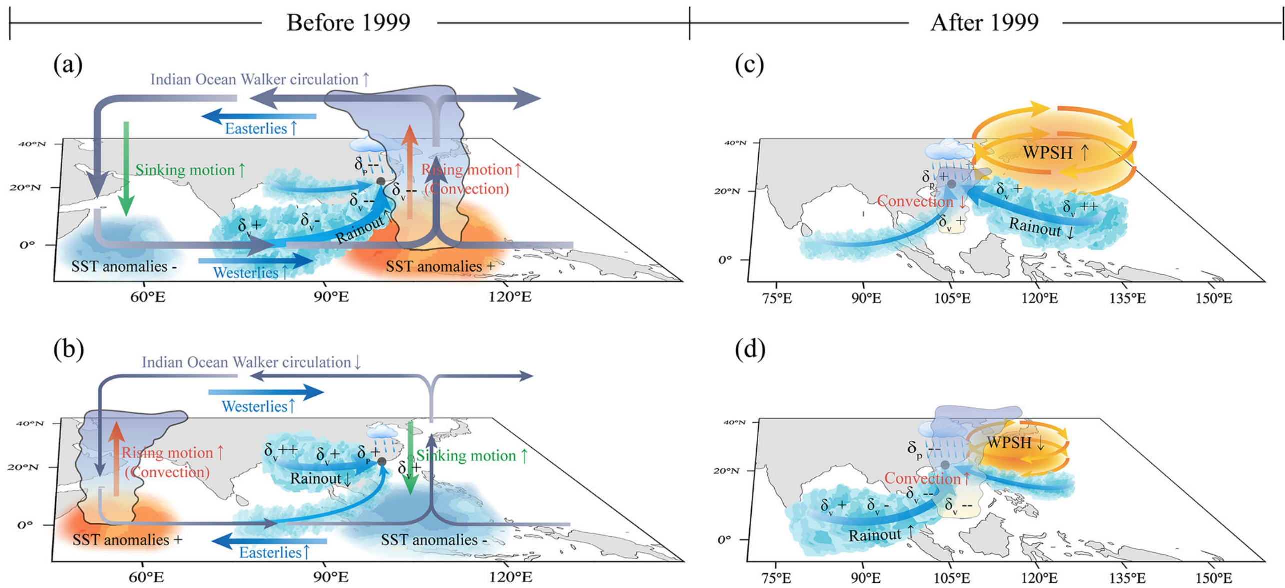

Fig. 4 | Schematic diagrams of the impacts of the IOD and WPSH on annual $\delta^{18}O_p$ in southern East Asia before and after 1999, respectively. a, b The impacts of the IOD on annual $\delta^{18}O_p$ in southern East Asia during the strongly negative (**a**) and positive (**b**) IOD years before 1999. **c, d** The impacts of the WPSH on annual $\delta^{18}O_p$ in southern East Asia during the extremely strong (**c**) and relatively weak (**d**) WPSH years after 1999. The δ_v indicates water vapor $\delta^{18}O$, and δ_p indicates $\delta^{18}O_p$. The plus (minus) signs indicate increased (decreased) δ and SST anomalies values, and the numbers of the plus (minus) signs indicate the magnitudes of those increases (decreases).

Impact of WPSH on annual $\delta^{18}O_p$

To investigate the changing influence of the WPSH on the annual $\delta^{18}O_p$ in southern East Asia before and after 1999, we analyzed the 500 hPa geopotential height anomalies during the two periods of 1961–1998 and 1999–2021, respectively (Supplementary Fig. 3). During 1961–1998, the 500 hPa geopotential height displays negative anomalies in the tropical and mid-latitude Pacific and forms an anomalously low-value center in the northern Pacific at about 37°N (Supplementary Fig. 3a). Correspondingly, the normalized WPSHII also displays frequent negative anomalies during this period (Supplementary Fig. 1b). These results indicate that the intensity of the WPSH was very weak in the 1961–1998 period. Therefore, during this period, the WPSH had negligible influence on the interannual variations of the $\delta^{18}O_p$ at Hong Kong and across southern East Asia. That is, the changes of the annual $\delta^{18}O_p$ in southern East Asia are independent of the changes of the WPSHII over the 1961–1998 period (Fig. 1c, f).

In contrast, the 500 hPa geopotential height during the 1999–2021 period displays positive anomalies in the tropical and mid-latitude Pacific and forms an anomalously high-value center in the northern Pacific (Supplementary Fig. 3b). In addition, the normalized WPSHII experiences an increasing trend and contains more frequent positive anomalies with very few negative anomalies during the 1999–2021 period (Supplementary Fig. 1b). These results indicate that the WPSH intensifies considerably during this period. Our results are consistent with previous studies finding an intensification of the WPSH during this period[59]. This intensification of the WPSH in the 1999–2021 period greatly influenced the interannual changes of the $\delta^{18}O_p$ across southern East Asia. In this case, the correlation between the interannual fluctuations of $\delta^{18}O_p$ across southern East Asia and the WPSHII between 1999 and 2021 becomes significant (Fig. 1c, g).

We then focus on the extremely strong (2010, 2016, and 2020) and relatively weak (2000 and 2012) WPSH years during the 1999–2021 period (the years were selected by the WPSHII in Supplementary Fig. 1b) to explore how the WPSH affects the annual $\delta^{18}O_p$ in southern East Asia. During the extremely strong WPSH years, the 500 hPa geopotential height field anomalies show a significant positive value center in the northern Pacific at about 30°N (Fig. 5a). The extremely strong WPSH expands westward and largely blocks the eastward transport of moisture from the Indian Ocean. This results in decreased moisture supply from the Indian Ocean (rectangles drawn with dashed pink lines in Fig. 5c, e). In comparison, this extremely strong WPSH drives a strong anticyclone circulation to form in the northwestern Pacific (110°E–180°, 0°–30°N) (Fig. 5c, e). The easterly winds on the south side of the anticyclone drove moisture from the northwestern Pacific westward, and the southerly winds on the west side of the anticyclone transported the moisture northwards to Hong Kong (ovals drawn with a solid pink line in Fig. 5c, e). Consequently, the moisture sourced from the northwestern Pacific and delivered to southern East Asia considerably increased in the extremely strong WPSH years (ovals drawn with a solid pink line in Fig. 5c, e). It is worth noting that the $\delta^{18}O_v$ in the northwestern Pacific is higher than in the Indian Ocean (Supplementary Fig. 4a), indicating the relatively high background $\delta^{18}O_v$. This can result in higher $\delta^{18}O_p$ values in southern East Asia. In addition, as more isotopically enriched moisture traveled a shorter distance and a relatively small latitude range from the northwestern Pacific to southern East Asia in the extremely strong WPSH years, the isotopic depletion was comparatively weaker and the $\delta^{18}O_p$ in southern East Asia is higher (Fig. 4c). Furthermore, the OLR values in the extremely strong WPSH years show positive anomalies in the Indo-Pacific Warm Pool (Fig. 6a), which imply a significantly weakened convection in this region. The weak convection along the transport pathway also contributes to the relatively high $\delta^{18}O_p$ values during the extremely strong WPSH years (Fig. 4c). As a result, the range of $\delta^{18}O_p$ values at Hong Kong extends from −4.27‰ to −5.11‰, with a mean of −4.76‰. (Figs. 1b, c and 4c).

In contrast, in the relatively weak WPSH years, the 500 hPa geopotential height displays negative anomalies (Fig. 5b). The WPSH weakens and retreats eastward, which has less power to drive moisture from the northwest Pacific to southern East Asia but allows moisture from the Indian Ocean to be transported almost unimpeded to southern East Asia. Consequently, the moisture supplied from the northwestern Pacific to southern East Asia is reduced (ovals drawn with a dashed pink line in Fig. 5d, f) with a larger amount of moisture derived from the southern Bay of Bengal and Indian Ocean (rectangle drawn with solid pink lines in Fig. 5d, f). Correspondingly, the lower $\delta^{18}O_v$ values from the southern Bay of Bengal and Indian Ocean (Supplementary Fig. 4b) contribute to the lower background values for the $\delta^{18}O_p$ in southern East Asia. In addition, the moisture from the southern Bay of Bengal and the Indian Ocean is transported to southern East Asia experiences a long transport pathway and an obvious latitude change, which cause a stronger isotopic depletion along the moisture transport pathway.

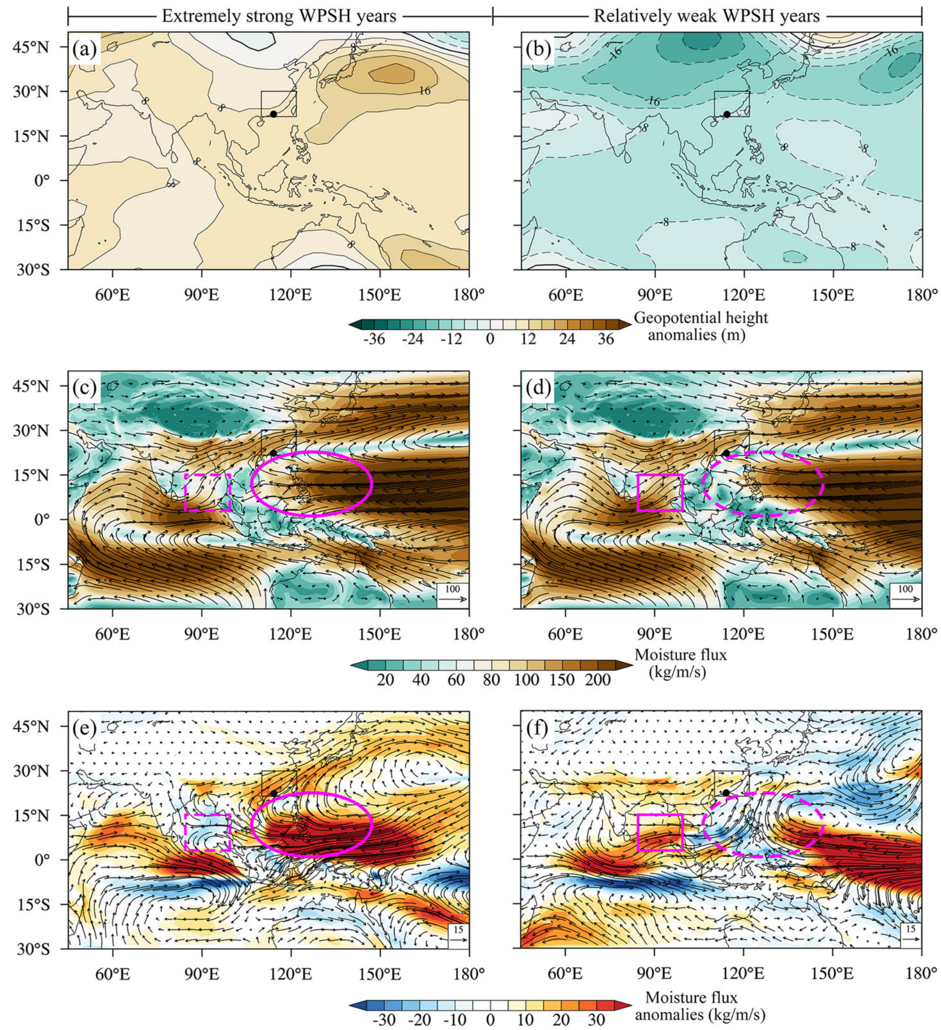

Fig. 5 | Geopotential height anomalies and atmospheric circulation patterns in the extremely strong and relatively weak WPSH years. **a**, **b** Annual 500 hPa geopotential height anomalies in the extremely strong (**a**) and relatively weak (**b**) WPSH years. **c**–**f** Vertically integrated moisture flux fields (**c**, **d**) and moisture flux field anomalies (**e**, **f**) at 1000–500 hPa in the extremely strong (**c**, **e**) and relatively weak (**d**, **f**) WPSH years. The anomalies are defined as the values in the extremely strong and relatively weak WPSH years subtracted by the mean values during 1999–2021, respectively. The black dots indicate the location of Hong Kong, and the black rectangles mark the region of southern East Asia. The solid (dashed) line circles or rectangles with pink in (**c**–**f**) mark the areas of increased (decreased) moisture flux.

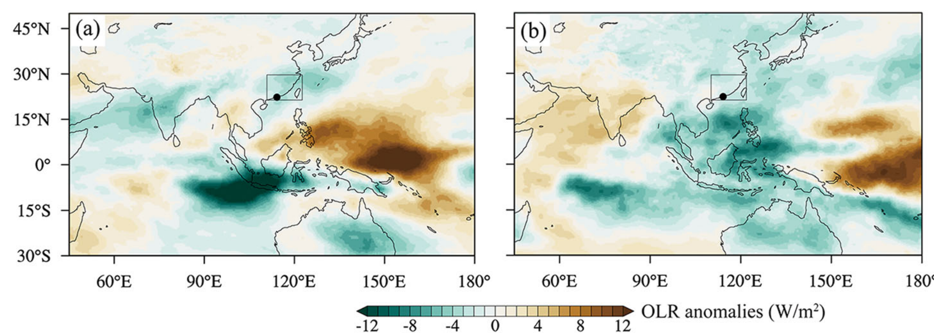

Fig. 6 | Spatial distributions of annual OLR anomalies during the extremely strong and relatively weak WPSH years. **a** The extremely strong WPSH years. **b** The relatively weak WPSH years. The black dots indicate the location of Hong Kong, and the black rectangles mark the region of southern East Asia.

These processes result in the lower $\delta^{18}O_p$ in southern East Asia (Fig. 4d). More importantly, in this case, convection obviously enhances in the Indo-Pacific warm Pool indicated by the negative anomalies of OLR (Fig. 6b). Therefore, when the moisture from the remote southern Bay of Bengal and Indian Ocean in the lower latitude is transported northward and passes through the Indo-Pacific Warm Pool, the significantly enhanced convection lifts moisture from near-surface to high altitude. The process further decreases the $\delta^{18}O_v$ and is responsible for the lower $\delta^{18}O_p$ in southern East Asia when the moisture is transported to this area in the relatively weak WPSH years (Fig. 4d). That is, the increasing moisture supply from the southern Bay of Bengal and the Indian Ocean, coupled with the enhanced convection, results in the lower values of annual $\delta^{18}O_p$ in southern East Asia (annual $\delta^{18}O_p$ values ranged from −5.27‰ to −6.03‰, with an average value being −5.65‰ at Hong Kong, which is 0.89‰ lower than during the extremely strong WPSH years) (Fig. 1b, c and 4d).

Discussion

This study investigated the relationships between the IOD/WPSH and the annual $\delta^{18}O_p$ at Hong Kong and even in the broader southern East Asia during 1961–2021. We found that both the IOD and WPSH influenced the interannual changes of $\delta^{18}O_p$ in this region, albeit over different periods, and that a major shift occurred around 1999. That is, the IOD played an important role on annual $\delta^{18}O_p$ in southern East Asia during 1961–1998 while the influence of the WPSH becomes important in the following 1999–2021 period.

Specifically, before 1999, the Indian Ocean Walker circulation strengthened during the strongly negative IOD years, which drove more moisture from the equatorial Indian Ocean to our study area. The isotopically depleted moisture supply resulted from the low background $\delta^{18}O_v$ values, the long transport pathway, and the large latitude difference, combined with the stronger convection, contributed to the lower $\delta^{18}O_p$ values in southern East Asia. However, the relatively high $\delta^{18}O_p$ values occurred in southern East Asia during the strongly positive IOD years, which were caused by the obviously increased moisture supply from the northern Bay of Bengal and the northern Indochina Peninsula and weaker convection in the Indo-Pacific Warm Pool. Meanwhile, the WPSH was very weak during this period and had little influence on the annual $\delta^{18}O_p$ in our study area.

After 1999, the symmetric pattern of the IOD changed to an asymmetric pattern, which effectively decoupled the linkage of the IOD and the annual $\delta^{18}O_p$ in southern East Asia. Hence, the annual $\delta^{18}O_p$ in southern East Asia "lost" the signal of the IOD. In contrast, the enhanced WPSH during this period significantly affected the interannual changes of $\delta^{18}O_p$ across southern East Asia. In other words, the annual $\delta^{18}O_p$ "retained" the WPSH signal. Therefore, the correlation between the annual $\delta^{18}O_p$ and the WPSH becomes significant, with the higher (lower) $\delta^{18}O_p$ values corresponding to the stronger (weaker) WPSH.

Our results highlight the important roles of the IOD and WPSH that influence the interannual variation of $\delta^{18}O_p$ across southern East Asia. We suggest that researchers need to consider the influences of the IOD and WPSH when interpreting paleoclimate archives. In particular, we found that a marked shift in the influences of the IOD and WPSH on the annual $\delta^{18}O_p$ in southern East Asia occurred around 1999. Hence, the influences of the IOD and WPSH on the annual $\delta^{18}O_p$ are likely to vary over different historical periods, and it may be necessary to interpret the paleo-$\delta^{18}O$ records within specific time segments.

In this study, we found that the transition of the IOD and the enhancement of the WPSH in 1999 resulted in shifting influences of the IOD and WPSH on the annual $\delta^{18}O_p$ across southern East Asia. Similarly, the effects of the WPSH on Asian monsoon precipitation and its teleconnection between India and northern China also changed around 1999[50,51]. What caused the changes in the IOD and WPSH around 1999 remains unclear and should be the subject of future research. It is noted that, on an interdecadal scale, the Pacific Decadal Oscillation (PDO) turned more negative also around 1999[60]. Therefore, it is worth exploring the possible relationships between the PDO and IOD/WPSH and verifying the trigger that caused the changes in the IOD and WPSH.

Methods

Study sites and stable isotope data

Hong Kong (114.17°E, 22.32°N, 66 m a.s.l.) resides within a typical monsoon climate region of southern East Asia (Fig. 1a). Mean air temperature between 1961 and 2021 at the site is relatively high at 23.1 °C. The annual air temperatures over this timeframe display small interannual differences ranging from 21.6 °C to 24.1 °C. The corresponding annual mean precipitation amount is about 2300 mm. In contrast to air temperature, precipitation amount has much higher interannual variability ranging from less than 1000 mm to over 3000 mm.

In this study, we first obtained the observed monthly $\delta^{18}O_p$ data at Hong Kong during 1961–2021 (data from 1966 to 1972 are missing) from the Global Network of Isotopes in Precipitation (GNIP). To analyze the interannual variability of $\delta^{18}O_p$, we then calculated the monthly $\delta^{18}O_p$ values to annual values. The $\delta^{18}O_p$ series from Hong Kong represents the longest observed record from East Asia and provides the foundation for revealing the links between annual $\delta^{18}O_p$ and atmospheric circulations.

In addition, we used the modeled $\delta^{18}O_p$ and water vapor $\delta^{18}O$ ($\delta^{18}O_v$) outputs from ECHAM6-wiso for the period 1979–2020[61,62]. ECHAM6 is the sixth generation of the general atmospheric circulation model ECHAM[63], and ECHAM6-wiso is its isotopic version. The 3D fields of temperature, vorticity, and divergence, as well as the surface pressure field of the ECHAM6-wiso simulation were nudged toward the ERA5 reanalysis dataset. The monthly mean sea surface temperature and sea-ice fields from the ERA5 reanalysis have been applied as ocean surface boundary conditions, too[64]. The ECHAM6-wiso has a relatively high spatial resolution (0.9° × 0.9° and 95 vertical levels) and a 6-h temporal resolution[62]. Details about the implementation of stable water isotopes in ECHAM6 have been described in Cauquoin et al.[61]. The modeled $\delta^{18}O_p$ data from ECHAM6-wiso at Hong Kong, are in good agreement with the observed $\delta^{18}O_p$ data from GNIP, with a significant and positive correlation of 0.77 ($n = 473, p < 0.01$) (Supplementary Fig. 5). Moreover, previous studies have also evaluated the ECHAM6-wiso data using various observational data from other regions[54,62], and found that ECHAM6-wiso results are in good agreement with the observations. Therefore, the ECHAM6-wiso model outputs can be used to confidently reproduce the variations in $\delta^{18}O_p$ across southern East Asia.

Atmospheric circulation indices

The IOD is a seesaw phenomenon of sea surface temperature (SST) anomalies that occurs between the eastern and western tropical Indian Oceans. The IOD intensity is indicated by the dipole mode index (DMI), which is calculated by the anomalous SST gradient between the western equatorial Indian Ocean (50°E–70°E and 10°S–10°N) and the southeastern equatorial Indian Ocean (90°E–110°E and 10°S–0°N). When DMI > 0, the phenomenon is known as the positive IOD phase, and when DMI < 0, it falls within the negative IOD phase. The DMI data are provided by the NOAA Physical Sciences Laboratory and are calculated based on the SST data from the United Kingdom Met Office Hadley Center Global Sea Ice and Sea Surface Temperature Dataset version 1 (HadISST1).

The WPSH located in the Pacific Ocean, is one of the most important atmospheric circulation systems, with the intensity changes of the WPSH indicated by the WPSH Intensity Index (WPSHII)[65]. The WPSHII is defined as the difference between the grid point's height exceeding 5880 and 5870 gpm multiplied by the sum of the total area encircled by the 5880 gpm isoline at 500 hPa within the region 10°N–60°N, 110°E–180°E[65]. The potential height data based on the NCEP/NCAR reanalysis datasets are used to calculate the WPSHII. The calculation formula[65] of the WPSHII is as follows:

$$WPSHII = dx \times dy \times \sum_i \sum_j \left(n_{ij} \times \left(H_{ij} - 5870 \right) \times \cos \varphi_j \right)$$

$$n_{ij} = \begin{cases} 1, \ H_{ij} \geq 5880 \\ 0, \ H_{ij} < 5880 \end{cases}$$

In the formula, dx is the distance value of the latitudinal grid point, and dy is the distance value of the meridional grid point; i is the ordinal number for the zonal grid point, $i = 1, 2, \ldots, n_x$, and n_x is the sum of grid points in the monitoring range, increasing from west to east; $j = 1, 2, \ldots, n_y$, and n_y is the sum of grid points in the monitoring range, increasing from south to north. H_{ij} is the potential height value of the grid point on the 500 hPa height field, and φ_j is the latitude value of the grid point.

The WPSHII data were obtained from the Climate Diagnostics and Prediction Division, National Climate Center, China Meteorological Administration. The relatively high values of the WPSHII indicate a strong WPSH, while relatively low values of WPSHII indicate a weak WPSH.

Meteorological data

In this study, we used outgoing longwave radiation (OLR) to indicate the intensity of convection. Note that the OLR data were calculated by the mean top net longwave radiation flux data. The vertical velocity data were also used to explore the vertical air motion anomalies. The moisture flux was calculated using a combination of the meteorological fields, including both eastward and northward wind components and the specific humidity on various pressure levels, and surface pressure on a single level. The total precipitation data were used to show the distributions of mean annual precipitation amount. We also used the geopotential height to evaluate the changes in WPSH. The meteorological data (1961–2021) mentioned above were obtained from the ERA5 reanalysis dataset provided by the European Center for Medium-

Range Weather Forecasts (ECWMF), with a spatial resolution of 0.25° × 0.25°. In addition, we used the SST data to reflect the interannual variations of SST anomalies. The SST data during the period 1961–2021 were obtained from the HadISST1, with a spatial resolution of 1° × 1°.

Data availability

Sources of the data used in this study are as follows: the observed δ18Op data at Hong Kong are available from the GNIP database (https://www.iaea.org/services/networks/gnip). The modeled δ18Op and δ18Ov data in southern East Asia were obtained from the ECHAM6-wiso used in Cauquoin and Werner[62]. The DMI data were provided by the NOAA Physical Sciences Laboratory (https://climexp.knmi.nl/selectindex.cgi?id=someone@somewhere). The WPSHII data can be downloaded from http://cmdp.ncc-cma.net. The SST data were obtained from HadISST1 (https://www.metoffice.gov.uk/hadobs/hadisst/data/download.html).
The ERA5 reanalysis data on single levels, including mean top net long-wave radiation flux, surface pressure, and total precipitation are available from https://cds.climate.copernicus.eu/cdsapp#!/dataset/reanalysis-era5-single-levels-monthly-means?tab=form. The ERA5 reanalysis data on pressure levels, including vertical velocity, eastward and northward wind components, specific humidity, and geopotential are available from https://cds.climate.copernicus.eu/cdsapp#!/dataset/reanalysis-era5-pressure-levels-monthly-means?tab=form.

Received: 15 August 2024; Accepted: 10 March 2025;
Published online: 17 March 2025

References

1. Huang, J., Yu, H., Dai, A., Wei, Y. & Kang, L. Drylands face potential threat under 2°C global warming target. *Nat. Clim. Change* **7**, 417–425 (2017).
2. Ning, G. et al. Rising risks of compound extreme heat-precipitation events in China. *Int. J. Climatol.* **42**, 5785–5795 (2022).
3. Trenberth, K. E., Fasullo, J. T. & Shepherd, T. G. Attribution of climate extreme events. *Nat. Clim. Change* **5**, 725–730 (2015).
4. Wang, B., Wu, R. & Li, T. Atmosphere–warm ocean interaction and its impacts on Asian–Australian monsoon variation. *J. Clim.* **16**, 1195–1211 (2003).
5. Tokinaga, H. et al. Regional patterns of tropical Indo-Pacific climate change: evidence of the Walker circulation weakening. *J. Clim.* **25**, 1689–1710 (2012).
6. Vecchi, G. A. et al. Weakening of tropical Pacific atmospheric circulation due to anthropogenic forcing. *Nature* **441**, 73–76 (2006).
7. Cheng, H. et al. The Asian monsoon over the past 640,000 years and ice age terminations. *Nature* **541**, 640–646 (2016).
8. Hu, J., Emile-Geay, J., Tabor, C., Nusbaumer, J. & Partin, J. Deciphering oxygen isotope records from Chinese speleothems with an isotope-enabled climate model. *Paleoceanogr. Paleoclimatol.* **34**, 2098–2112 (2019).
9. Wang, Y. et al. A high-resolution absolute-dated late Pleistocene Monsoon record from Hulu Cave, China. *Science* **294**, 2345–2348 (2001).
10. Liu, X. et al. A shift in cloud cover over the southeastern Tibetan Plateau since 1600: evidence from regional tree-ring δ^{18}O and its linkages to tropical oceans. *Quat. Sci. Rev.* **88**, 55–68 (2014).
11. Liu, Y. et al. Recent enhancement of central Pacific El Niño variability relative to last eight centuries. *Nat. Commun.* **8**, 15386 (2017).
12. Preechamart, S. et al. Tree-ring oxygen isotope chronology of teak log coffins in northwestern Thailand and its relationship with Pacific Decadal Oscillation and El Niño-Southern Oscillation. *Quatern. Int.* **629**, 81–92 (2022).
13. Xu, C. et al. Decreasing Indian summer monsoon on the northern Indian sub-continent during the last 180 years: evidence from five tree-ring cellulose oxygen isotope chronologies. *Climate* **14**, 653–664 (2018).
14. Jiang, L. et al. Modulation of East Asian monsoon strength by ENSO during the warm periods of the late Holocene: Evidence from Porites corals in the northern South China Sea. *Glob. Planet. Change* **225**, 104136 (2023).
15. Watanabe, T. et al. Permanent El Niño during the Pliocene warm period not supported by coral evidence. *Nature* **471**, 209–211 (2011).
16. Watanabe, T., Kawamura, T., Yamazaki, A., Murayama, M. & Yamano, H. A 106 year monthly coral record reveals that the East Asian summer monsoon modulates winter PDO variability. *Geophys. Res. Lett.* **41**, 3609–3614 (2014).
17. Chakraborty, S. et al. Linkage between precipitation isotopes and biosphere-atmosphere interaction observed in northeast India. *npj Clim. Atmos. Sci.* **5**, 10 (2022).
18. Jeelani, G., Deshpande, R. D., Galkowski, M. & Rozanski, K. Isotopic composition of daily precipitation along the southern foothills of the Himalayas: impact of marine and continental sources of atmospheric moisture. *Atmos. Chem. Phys.* **18**, 8789–8805 (2018).
19. Kurita, N., Fujiyoshi, Y., Nakayama, T., Matsumi, Y. & Kitagawa, H. East Asian Monsoon controls on the inter-annual variability in precipitation isotope ratio in Japan. *Climate* **11**, 339–353 (2015).
20. Lekshmy, P. R., Midhun, M. & Ramesh, R. Spatial variation of amount effect over peninsular India and Sri Lanka: Role of seasonality. *Geophys. Res. Lett.* **42**, 5500–5507 (2015).
21. Sinha, N. & Chakraborty, S. Isotopic interaction and source moisture control on the isotopic composition of rainfall over the Bay of Bengal. *Atmos. Res.* **235**, 104760 (2020).
22. Wei, Z. et al. Influences of large-scale convection and moisture source on monthly precipitation isotope ratios observed in Thailand, Southeast Asia. *Earth Planet. Sci. Lett.* **488**, 181–192 (2018).
23. Yu, W. et al. Precipitation stable isotope records from the northern Hengduan Mountains in China capture signals of the winter India-Burma Trough and the Indian Summer Monsoon. *Earth Planet. Sci. Lett.* **477**, 123–133 (2017).
24. Zhan, Z. et al. Determining key upstream convection and rainout zones affecting δ^{18}O in water vapor and precipitation based on 10-year continuous observations in the East Asian Monsoon region. *Earth Planet. Sci. Lett.* **601**, 117912 (2023).
25. Zhang, J. et al. Coupled effects of moisture transport pathway and convection on stable isotopes in precipitation in East Asia: Implications for paleoclimate reconstruction. *J. Clim.* **24**, 9811–9822 (2021).
26. Aggarwal, P. K., Fröhlich, K., Kulkarni, K. M. & Gourcy, L. L. Stable isotope evidence for moisture sources in the Asian summer monsoon under present and past climate regimes. *Geophys. Res. Lett.* **31**, L08203 (2004).
27. Tang, Y. et al. Using stable isotopes to understand seasonal and interannual dynamics in moisture sources and atmospheric circulation in precipitation. *Hydrol. Process.* **31**, 4682–4692 (2017).
28. Wang, Y., Hu, C., Ruan, J. & Johnson, K. R. East Asian precipitation δ18O relationship with various monsoon indices. *J. Geophys. Res. Atmos.* **125**, e2019JD032282 (2020).
29. Wu, H. et al. Atmospheric processes control the stable isotopic variability of precipitation in the middle–lower reaches of the Yangtze River Basin, East Asian monsoon region. *J. Hydrol.* **623**, 129835 (2023).
30. Yang, H., Johnson, K. R., Griffiths, M. L. & Yoshimura, K. Interannual controls on oxygen isotope variability in Asian monsoon precipitation and implications for paleoclimate reconstructions. *J. Geophys. Res. Atmos.* **121**, 8410–8428 (2016).
31. Yang, X., Davis, M. E., Acharya, S. & Yao, T. Asian monsoon variations revealed from stable isotopes in precipitation. *Clim. Dyn.* **51**, 2267–2283 (2017).
32. Duy, N. L., Heidbüchel, I., Meyer, H., Merz, B. & Apel, H. What controls the stable isotope composition of precipitation in the Mekong Delta? A model-based statistical approach. *Hydrol. Earth Syst. Sci.* **22**, 1239–1262 (2018).
33. Li, Y., Rao, Z., Cao, J., Jiang, H. & Gao, Y. Highly negative oxygen isotopes in precipitation in southwest China and their significance in paleoclimatic studies. *Quatern. Int.* **440**, 64–71 (2017).

34. Li, Y., Liu, X., Xie, X., Cauquoin, A. & Werner, M. Interannual modulation of the East and South Asian summer precipitation $\delta^{18}O$ by the Indian and western North Pacific summer monsoon strength. *Glob. Planet. Change* **227**, 104187 (2023).
35. Tan, M. Circulation effect: response of precipitation $\delta^{18}O$ to the ENSO cycle in monsoon regions of China. *Clim. Dyn.* **42**, 1067–1077 (2014).
36. Chiang, J. C. H., Herman, M. J., Yoshimura, K. & Fung, I. Y. Enriched East Asian oxygen isotope of precipitation indicates reduced summer seasonality in regional climate and westerlies. *Proc. Natl Acad. Sci. USA* **117**, 14745–14750 (2020).
37. Falster, G., Konecky, B., Madhavan, M., Stevenson, S. & Coats, S. Imprint of the Pacific Walker Circulation in Global Precipitation $\delta^{18}O$. *J. Clim.* **34**, 579–8597 (2021).
38. Ishizaki, Y. et al. Interannual variability of $H_2{}^{18}O$ in precipitation over the Asian monsoon region. *J. Geophys. Res.* **117**, D16308 (2012).
39. Liu, Z. et al. The relations between summer droughts/floods and oxygen isotope composition of precipitation in the Dongting Lake basin. *Int. J. Climatol.* **43**, 3590–3604 (2023).
40. Cai, Z., Tian, L. & Bowen, G. J. ENSO variability reflected in precipitation oxygen isotopes across the Asian Summer Monsoon region. *Earth Planet. Sci. Lett.* **475**, 25–33 (2017).
41. Permana, D. S., Thompson, L. G. & Setyadi, G. Tropical West Pacific moisture dynamics and climate controls on rainfall isotopic ratios in southern Papua, Indonesia. *J. Geophys. Res. Atmos.* **121**, 2222–2245 (2016).
42. Ruan, J., Zhang, H., Cai, Z., Yang, X. & Yin, J. Regional controls on daily to interannual variations of precipitation isotope ratios in Southeast China: Implications for paleomonsoon reconstruction. *Earth Planet. Sci. Lett.* **527**, 115794 (2019).
43. He, S. et al. Understanding tropical convection through triple oxygen isotopes of precipitation from the maritime continent. *J. Geophys. Res. Atmos.* **126**, e2020JD033418 (2021).
44. Cai, Z., Tian, L. & Bowen, G. J. Influence of recent climate shifts on the relationship between ENSO and Asian Monsoon precipitation oxygen isotope ratios. *J. Geophys. Res. Atmos.* **124**, 7825–7835 (2019).
45. Hrudya, P. P. V. H., Varikoden, H. & Vishnu, R. N. Changes in the relationship between Indian Ocean Dipole and Indian summer monsoon rainfall in early and recent multidecadal epochs during different phases of monsoon. *Int. J. Climatol.* **41**, E305–E318 (2020).
46. Qiu, Y., Cai, W., Guo, X. & Ng, B. The asymmetric influence of the positive and negative IOD events on China's rainfall. *Sci. Rep.* **4**, 4943 (2014).
47. Takaya, Y., Ishikawa, I., Kobayashi, C., Endo, H. & Ose, T. Enhanced Meiyu-Baiu rainfall in early summer 2020: Aftermath of the 2019 super IOD event. *Geophys. Res. Lett.* **47**, e2020GL090671 (2020).
48. Cai, W. et al. Increased frequency of extreme Indian Ocean Dipole events due to greenhouse warming. *Nature* **510**, 254–258 (2014).
49. Cai, W. et al. Opposite response of strong and moderate positive Indian Ocean Dipole to global warming. *Nat. Clim. Change* **11**, 27–32 (2021).
50. Huang, Y., Wang, B., Li, X. & Wang, H. Changes in the influence of the western Pacific subtropical high on Asian summer monsoon rainfall in the late 1990s. *Clim. Dyn.* **51**, 443–455 (2018).
51. Li, S., Liu, L., Gong, Z., Yang, J. & Feng, G. The Enhancement of the Summer Precipitation Teleconnection between India and the Northern Part of Eastern China after the Late 1990s. *J. Clim.* **36**, 3043–3062 (2023).
52. Zhou, T. et al. Why the western Pacific subtropical high has extended westward since the late 1970s. *J. Clim.* **22**, 2199–2215 (2009).
53. Feng, X., Faiia, A. M. & Posmentier, E. S. Seasonality of isotopes in precipitation: a global perspective. *J. Geophys. Res. Atmos.* **114**, D08116 (2009).
54. Zhang, J. et al. Controls on stable water isotopes in monsoonal precipitation across the Bay of Bengal: Atmosphere and surface analysis. *Geophys. Res. Lett.* **50**, e2022GL102229 (2023).
55. He, C. & Zhou, T. Responses of the western North Pacific subtropical high to global warming under RCP4.5 and RCP8.5 scenarios projected by 33 CMIP5 models: the dominance of tropical Indian ocean–tropical western Pacific SST gradient. *J. Clim.* **28**, 365–380 (2015).
56. Yang, K. et al. Increased variability of the western Pacific subtropical high under greenhouse warming. *Proc. Natl Acad. Sci. USA* **119**, e2120335119 (2022).
57. Kurita, N. Water isotopic variability in response to mesoscale convective system over the tropical ocean. *J. Geophys. Res. Atmos.* **118**, 10376–10390 (2013).
58. Lekshmy, P. R., Midhun, M. & Ramesh, R. Role of moisture transport from Western Pacific region on water vapor isotopes over the Bay of Bengal. *Atmos. Res.* **265**, 105895 (2022).
59. Matsumura, S., Sugimoto, S. & Sato, T. Recent intensification of the western Pacific subtropical high associated with the East Asian summer monsoon. *J. Clim.* **28**, 2873–2883 (2015).
60. Yang, L., Chen, S., Wang, C., Wang, D. & Wang, X. Potential impact of the Pacific Decadal Oscillation and sea surface temperature in the tropical Indian Ocean–Western Pacific on the variability of typhoon landfall on the China coast. *Clim. Dyn.* **51**, 2695–2705 (2018).
61. Cauquoin, A., Werner, M. & Lohmann, G. Water isotopes—climate relationships for the mid-Holocene and preindustrial period simulated with an isotope-enabled version of MPI-ESM. *Climate* **15**, 1913–1937 (2019).
62. Cauquoin, A. & Werner, M. High-resolution nudged isotope modeling with ECHAM6-wiso: Impacts of updated model physics and ERA5 reanalysis data. *J. Adv. Model. Earth Syst.* **13**, e2021MS002532 (2021).
63. Stevens, B. et al. Atmospheric component of the MPI-M Earth System Model: ECHAM6. *J. Adv. Model. Earth Syst.* **5**, 146–172 (2013).
64. Hersbach, H. et al. The ERA5 global reanalysis. *Q. J. Roy. Meteor. Soc.* **146**, 1999–2049 (2020).
65. Liu, Y., Liang, P. & Sun, Y. *The Asian summer monsoon: characteristics, variability, teleconnections and projection* (eds Liu, Y. et al.) 85–95 (Elsevier, 2019).

Acknowledgements
This work was funded by the Second Tibetan Plateau Scientific Expedition and Research Program (2024QZKK0400), the Basic Science Center for Tibetan Plateau Earth System (BSCTPES, NSFC project no. 41988101-03), the National Natural Science Foundation of China (42171122), and the China Postdoctoral Science Foundation (2023M733607).

Author contributions
J.Z. analyzed data, produced figures, and wrote the draft of the paper. W.Y. designed the study, discussed the results, edited the paper, and provided the funding acquisition. L.G.T. and S.L. discussed the results and edited the paper. A.C. and M.W. provided data and edited the paper. Z.J., Y.M., B.X., G.W., R.G., P.R., Z.Z., Q.W., and D.Q. edited the paper.

Competing interests
The authors declare no competing interests.

Additional information
Supplementary information The online version contains supplementary material available at https://doi.org/10.1038/s41612-025-01000-4.

Correspondence and requests for materials should be addressed to Wusheng Yu.